Journal of Solid State Electrochemistry (2019) 23:1767–1777
https://doi.org/10.1007/s10008-019-04256-y

ORIGINAL PAPER

Study on the fabrication and photoelectrochemical performance of the F^- doped Ti/Co_3O_4 electrodes with *n*-type semiconductor characteristics

Hongchao Ma[1] · Xiaoqin Wang[1] · Yinghuan Fu[1,2] · Yanan Zhang[1] · Chun Ma[1] · Xiaoli Dong[1] · Zhihui Yu[1,2]

Received: 23 October 2018 / Revised: 21 March 2019 / Accepted: 22 March 2019 / Published online: 8 May 2019

Abstract

Herein, the Ti/Co_3O_4 electrodes with n-type semiconductor characteristics were fabricated by a typical hydrothermal process using F^- ion as dopant, and their morphology control was also performed by tailoring the hydrothermal temperature. The F^- doped Ti/Co_3O_4 electrodes could be used as photoanode to degrade anthraquinone dye (reactive Brilliant Blue KN-R), and showed excellent photoelectrocatalytic (PEC) activity. It is proposed that the fast ions and electron transportation, high oxygen evolution potential, lower resistance, large active area, and good electrolyte infiltration are responsible for the improved PEC activity of the F^- doped Ti/Co_3O_4 system. Nevertheless, the F^- doped Ti/Co_3O_4 electrode with divergent flower-like structure composed of needle nanowires exhibited highest PEC activity than that of other electrodes. It is noteworthy that the presence of electrostatic anti-barrier arises from an "ohmic" contact between the metal (Ti) and the semiconductor (Co_3O_4) is also an important factor for the higher PEC activity of the F^- doped Ti/Co_3O_4 electrodes. The work provides unique insight into the design of Co_3O_4 photoanode from a perspective of tailoring the ion doping and morphology.

Keywords Photoelectrochemical oxidation · Co_3O_4 nanostructures · Photoanode · Anthraquinone dye

Introduction

In recent years, the electrochemical oxidation as an advanced oxidation technology has caused considerable attention in degradation of toxic or stubborn organic wastewater [1]. The so-called electrocatalytic oxidation technology containing a series of chemical reactions, electrochemical processes, or physical processes is carried in a specific electrochemical reactor to achieve the desired purpose design using an external power plant [2]. Compared with conventional treatment methods, electrocatalytic oxidation technology is versatile, and that the reaction process is easy to measure and control [3]. The •OH radicals derived from water electrolysis can react directly with organic contaminants to form carbon dioxide in wastewater. The electrochemical equipment is relatively simple and has many unique functions such as flotation, flocculation, and sterilization. It can be used as a treating unit or combined with other methods [4–6]. However, the practical application of electrochemical oxidation techniques depends on the use of suitable anode with long service life, high activity, and low cost in the treatment of organic wastewater. Many materials have been used as anodes, such as RuO_2 [7], SnO_2 [8, 9], PbO_2 [10], and boron-doped diamond (BDD) [11] due to their high oxygen evolution potential which can effectively suppress the side effects of oxygen evolution and improve the production of hydroxyl radicals [12–16].

To remove the organic pollutants in wastewater more efficiently, some strategies have been done to promote electrooxidation process via modification of electrodes (doping of non-metal and metal elements [17, 18], heterostructure construction [19], noble metal particle decoration [19, 20]), development of new materials [21], and photoelectrocatalysis (PEC) process

✉ Yinghuan Fu
fuyinghuan@sina.com

✉ Zhihui Yu
2653260196@qq.com

[1] School of Light Industry and Chemical Engineering, Dalian Polytechnic University, No.1 Qinggongyuan, Ganjinzi District, Dalian, People's Republic of China

[2] School of Chemistry Engineering and Material, Dalian Polytechnic University, No.1 Qinggongyuan, Ganjinzi District, Dalian 116034, People's Republic of China

[22, 23]). Recently, PEC has been paid more attention as a simple and effective way to overcome the rapid recombination of photoinduced carriers by applying a positive bias potential. However, previous PEC studies can actually be considered as electro-assisted photocatalysis regarding the photocatalyst [24], and the electro-oxidation process has not attracted more attention. Some studies indicated the combination of electrocatalysis and photocatalysis would be more beneficial to increase the degradation efficiency of toxic or recalcitrant organics [7, 25]. Thus, the development of new materials containing photooxidation and electro-oxidation properties has become a major challenge in the field of photoelectrocatalysis.

Co_3O_4 is a very promising photocatalysis and electrocatalysis material for numerous applications in PEC reduction of CO_2, water oxidation, photocatalytic removal of organic pollutants, pseudo-capacitive material for super-capacitors, and so on [26–34]. Thus, Co_3O_4 can be considered as an attractive candidate to achieve the coupling of electro-oxidation and photo-oxidation. Nevertheless, the Co_3O_4 as photoanode material is unsuitable to degrade organic pollutants because the conventional Co_3O_4 is a *p*-type semiconductor. It is well known that the introduction of F^- not only can promote the morphology of the oxides, but also can convert the intrinsic semiconductor to *n*-type (e.g., SnO_2) [35–37]. Moreover, the presence of F^- in the crystal plays a key role in reducing the denucleation rate and activating the substrate, which leads to the strong mechanical adhesion between the nano-architecture and the substrate.

Based on above mentions, the F^- doped Co_3O_4 hierarchical microstructures were fabricated on the titanium substrate and used as expected semiconductor photoanode with *n*-type characteristics in this work. The as-obtained F^- doped Ti/Co_3O_4 photoanode showed the characteristics of *n*-type semiconductor, good decolorization efficiency and stability for degrading anthraquinone dye (reactive Brilliant Blue KN-R).

Experimental section

Materials

Titanium sheets (99.7% purity) were purchased from Yunjiemetal (China). The main chemicals were cobalt nitrate, urea, ammonium fluoride, anhydrous sodium sulfate, and reactive Brilliant Blue KN-R from Tianjin Chemical Reagent Company. All chemicals are analytical grade and can be used without further purification. Deionized water was used for all solution preparation.

Electrode preparation

A Ti sheet (10 mm × 10 mm × 1 mm) was used as a substrate. First, Ti sheets were cleaned in acetone and ethanol under ultrasonication, subsequently immersed in an aqueous oxalic acid solution (10%) for 2 h, and then washed using deionized water. Two millimolar $Co_2(NO)_3$, 10 mmol urea, and 5 mmol NH_4F were dissolved in 40 mL of deionized water and stirring vigorously for 20 min to obtain a slight pink solution. Then, the solution was moved into a PTFE autoclave (capacity of 60 mL) with etched titanium sheets. The hydrothermal reaction was performed at 80 °C, 90 °C, 120 °C, 150 °C, and 180 °C for 5 h, respectively. After the completion of the hydrothermal reaction, the titanium sheets with pink precursors were obtained. The as-obtained titanium sheets were rinsed with deionized water for 2–3 times, and then placed in a drying cabinet for 3 h. After drying, the samples were placed into a muffle furnace and calcined at 400 °C for 2 h with the heating speed of 2 °C min^{-1}. After cooling to room temperature, the F^- doped Ti/Co_3O_4 electrodes were obtained, and labeled as Ti/F-Co_3O_4-80 °C, Ti/F-Co_3O_4-90 °C, Ti/F-Co_3O_4-120 °C, Ti/F-Co_3O_4-150 °C, and Ti/F-Co_3O_4-180 °C, respectively.

For comparison, the Ti/Co_3O_4 reference was prepared via the same procedure as that of the F^- doped Ti/F-Co_3O_4-90 °C; only NH_4F was absent in the process.

Catalytic oxidation

The photoelectrocatalytic activity of the electrodes was evaluated by degradation of an anthraquinone dye solution (reactive Brilliant Blue KN-R, 60 mgL^{-1}, 200 mL). 0.1 M Na_2SO_4 solution was used as a supporting electrolyte in a quartz reactor. Titanium-based electrode loaded with Co_3O_4 and blank titanium sheet was used as anode and cathode, respectively. The anode and cathode are placed perpendicular, and parallel to each other with a distance of 3 cm. Electro-oxidation experiments were performed with a DC current source at a constant current density of 35 mA cm^{-2}. The light irradiation of the electrode for photocatalytic treatment was performed with a 10 W xenon lamp. The cooling of the reaction vessel is performed by using a circulating water jacket (a xenon lamp placed inside the jacket). In the experiment, samples were taken out of the reactor periodically and then analyzed.

Characterizations

Electrochemical measurements were recorded using a CHI 660E potentiostat/galvanostat (Chenhua Instruments, Shanghai, China) equipped with a three-electrode single compartment cell. Platinum plates and KCl-saturated calomel electrode (0.2415 V vs. SHE) were used as the counter and reference electrodes, respectively (it should be noted that the measured potential in our electrochemical experiment may deviate from the actual value because we did not use Luggin capillary to eliminate or minimize $iR_{solution}$ potential drop between the reference electrode and the working electrode. Nevertheless, it still is acceptable to compare the performance of electrodes

under same conditions). The morphologies of the electrode were characterized using a Hitachi-1510 scanning electron microscope (SEM) (Hitachi, Japan) and the transmission electron micrographs (TEM) (JEOL, JEM-2100). X-ray diffraction (XRD) analysis of the samples was performed on a SHIMADZU XRD-6100 X-ray diffractometer using Cu Kα radiation ($\lambda = 0.15406$ nm) as X-ray source, operated at 40 kV and 30 mA. Hall-effect measurements were performed in a magnetic field between 0.1 and 0.5 T at 300 K with a six-probe contact configuration (Hall Effect Measurement System ET9000, Eastchanging) using the van der Pauw method [38]. Field reversal was effectively performed by rotating the sample. The UV–vis diffuse reflectance spectra of samples were determined by a spectrophotometer (Varian Cary-100) and barium sulfate was used as a standard. Furthermore, the amount of O_3 generated in the photoelectrocatalytic process is identified by ultraviolet spectra analysis of blank solution (without anthraquinone dye) at 254 nm.

As previously reported, amount of ·OH (from the electrocatalytic decomposition of water on the electrode surface) could be detected using the analysis of the fluorescence spectra (benzoic acid had a known reaction with ·OH in aqueous media and the product is *p*-hydroxybenzoic acid (*p*-HBA). The *p*-HBA could be detected using fluorescence spectroscopy due to the existence of its characteristic peak at 440 nm). To investigate the amount of hydroxyl radical (·OH), the electrolysis of benzoic acid solution was performed in the present work. Initial concentration of benzoic acid is 200 mg L^{-1} and 0.5 mol L^{-1} Na_2SO_4 was used as a supporting electrolyte. During electrolysis, the sample was collected and analyzed at a desired time interval. The fluorescence spectra of solution were measured with excitation at 325 nm by a fluorescence spectrophotometer (Hitachi F-7000, Japan).

Results and discussion

To investigate the crystal structure and composition of the as-prepared electrodes, the X-ray diffraction analysis of the as-prepared electrodes was carried out. Figure 1 shows the XRD patterns of the samples prepared by hydrothermal method at temperatures ranged from 80 to 180 °C. As shown in Fig. 1, besides the typical diffraction peaks of metal Ti substrate (JCPDS card number 44-1294), only a weak diffraction peak of Co_3O_4 (JCPDS card number 65-3103) at 36.8° can be observed when hydrothermal temperature is 80 °C. As hydrothermal temperature increases, the peaks of (111), (220), (311), (400), (511), and (440) crystal face located at 19.0°, 31.3°, 36.8°, 44.8°, 59.4°, and 65.2° appeared gradually, and their intensity enhanced as well. XRD results indicated that the Co_3O_4 gradually grew on the surface of Ti substrate as enhancing hydrothermal temperature. Furthermore, it can be seen from Fig. 1 b and c that introducing F ions did not change the crystal structure of Co_3O_4.

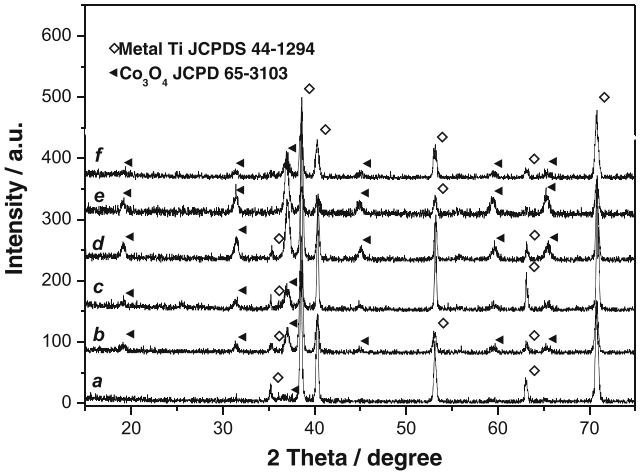

Fig. 1 XRD of samples prepared by hydrothermal conditions (a) Ti/F-Co_3O_4-80 °C, (b) Ti/Co_3O_4-reference, (c) Ti/F-Co_3O_4-90 °C, (d) Ti/F-Co_3O_4-120 °C, (e) Ti/F-Co_3O_4-150 °C, (f) Ti/F-Co_3O_4-180 °C

Figure 2 shows the images of scanning electron microscope (SEM) for the etched Ti sheet and the Ti/Co_3O_4 electrodes. As shown in Fig. 2 a, the surface of etched Ti sheet is a porous structure, and the porous size of Ti sheet is about 2–10 μm. It can be clearly seen from Fig. 2 b–g that large-scale cobalt oxide with various micro-structures directly grew on the porous surface of the Ti sheet when the porous Ti sheet underwent a hydrothermal treatment in Co^{3+} mother liquor under different temperatures. The SEM images of Ti sheet after hydrothermal treatment at 80 °C are shown in Fig. 2 b. It is found that the large amount of urchin-like Co_3O_4 architectures uniformly covered the surface of the substrate, and the size of these urchin-like Co_3O_4 is about 1.0 μm. When the hydrothermal temperature achieved to 90 °C, these urchin-like Co_3O_4 architectures are converted to divergent flower-like structure composed of needle nanowires with several micrometers in length (see Fig. 2c). To further enhance hydrothermal temperature, the surface of Ti substrate is densely covered by needle Co_3O_4 nanowires. The high-magnification SEM images further demonstrated that each Co_3O_4 nanowire is composed of numerous nanoparticles, and had average diameters of about 200 nm with around several micrometers in length (see Fig. 2d insets). It can be seen from Fig. 2 e that the neighboring nanowires stuck together in cluster under higher hydrothermal temperature (150 °C). As the hydrothermal temperature enhanced to 180 °C, the clustered Co_3O_4 nanowires subsequently converted to solid prisms (see Fig. 2f). As a comparison, the SEM observation of Ti/Co_3O_4 reference was also performed and shown in Fig. 2 g. It is noteworthy that Co_3O_4 sample without F^- doping is unordered nanowires, and densely covered on the surface of Ti substrate.

In order to study the surface information of the as-prepared electrodes, X-ray photoelectron spectroscopy (XPS) analysis

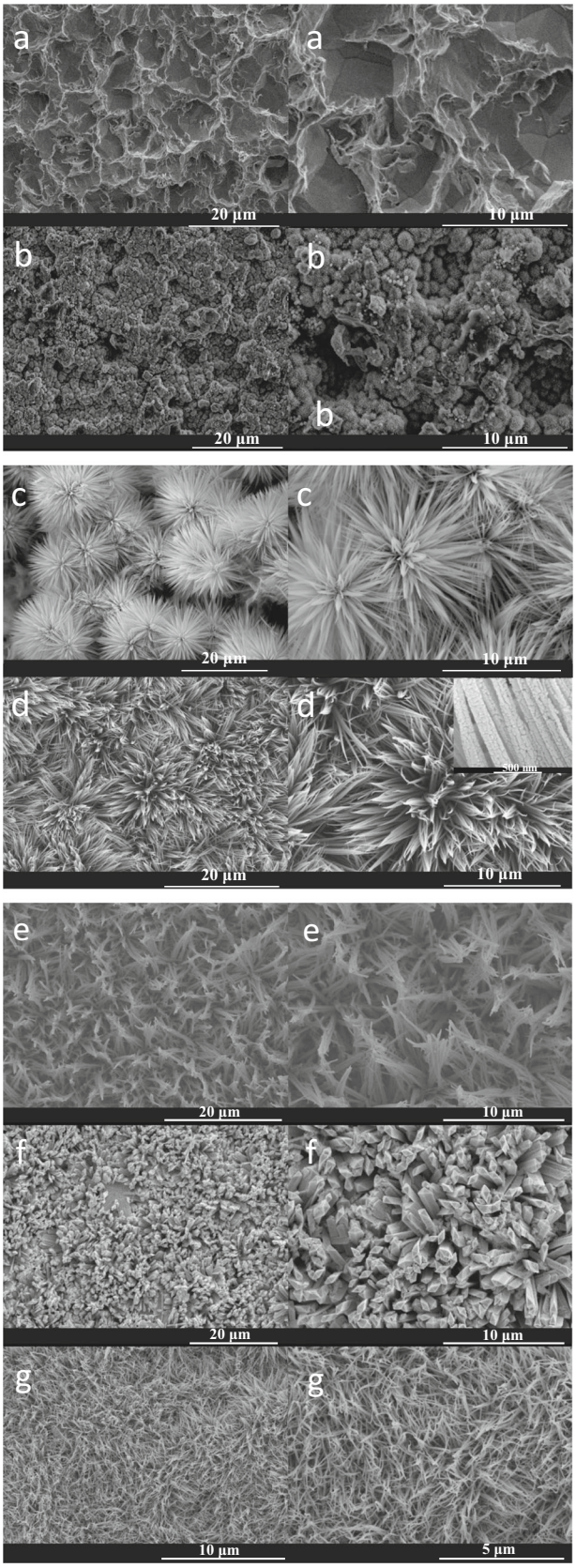

Fig. 2 SEM observations of samples (a) etched titanium sheet, (b) Ti/F-Co_3O_4-80 °C, (c) Ti/F-Co_3O_4-90 °C, (d) Ti/F-Co_3O_4-120 °C, (e) Ti/F-Co_3O_4-150 °C, (f) Ti/F-Co_3O_4-180 °C, (g) Ti/Co_3O_4-reference

was performed. The XPS spectra of the Ti/Co_3O_4 electrodes with or without F^- doping prepared by hydrothermal route at 90 °C were shown in Fig. 3. As shown in the full survey spectra (see Fig. 3a), element F could only be detected in the F^- doped Ti/Co_3O_4 electrode, which indicated that F ions were successfully introduced onto the Co_3O_4 coatings. The high-resolution Co2p XPS spectra (Fig. 3b) of both samples showed that the $Co2p_{3/2}$ and $Co2p_{1/2}$ peaks are located at 777.7 eV and 792.8 eV, respectively. Moreover, the gap between $Co2p_{3/2}$ and $Co2p_{1/2}$ peaks is about 15.1 eV, which confirms the Co oxide loaded on the Ti substrate is Co_3O_4 in both samples [39, 40]. The high-resolution spectra of the F1s region for both samples were displayed in Fig. 3 c. It can be seen that the distinct F1s peak could be observed for the F^- doped Ti/Co_3O_4 electrode, while no F1s signal was detected for the Ti/Co_3O_4 reference. As shown in Fig. 3 c, the F1s peak was located at 684.5 eV, indicating that the presence of lattice F^- substitutes oxygen atoms in the Co_3O_4 network arising from the incorporation of F^- species [41, 42].

To identify major conduction type, the measurements of the Hall coefficient for Ti/Co_3O_4 electrodes were performed. As shown in Fig. 4 a, the positive sign of Hall coefficients demonstrated the *p*-type conduction of the Ti/Co_3O_4 reference. On the contrary, the Hall coefficient of the F^- doped Ti/Co_3O_4 electrode was found to be negative, which clearly indicated that the conduction of the F^- doped Ti/Co_3O_4 is *n*-type. Furthermore, the Mott-Schottky plots of the Ti/Co_3O_4 reference showed a negative slope, which indicated the Ti/Co_3O_4 reference is a *p*-type semiconductor (see Fig. 4b). However, the Mott-Schottky plots of the F^- doped Ti/Co_3O_4 electrode showed a positive slope, confirming that the F^- doped Ti/Co_3O_4 electrode is an *n*-type semiconductor.

The Mott-Schottky plots of the F^- doped Ti/Co_3O_4 electrodes were shown in Fig. 5 a. The positive slope of the curves for the F^- doped Ti/Co_3O_4 electrodes indicated their characteristics of *n*-type semiconductors. It is well known that more negative flat band potential (E_{fb}) is believed to have better catalytic activity for an *n*-type semiconductor [43–45]. The flat band potentials of the F^- doped Ti/Co_3O_4 electrodes were determined to be − 0.425 V (Ti/F-Co_3O_4-180 °C), − 0.598 V (Ti/F-Co_3O_4-80 °C), − 0.683 V (Ti/F-Co_3O_4-150 °C), − 0.831 V (Ti/F-Co_3O_4-120 °C), and − 0.916 V (Ti/F-Co_3O_4-90 °C), respectively. Thus, the Ti/F-Co_3O_4-90 °C sample will exhibit better electrocatalytic activity than other Ti/F-Co_3O_4 electrodes. Furthermore, the carrier concentration (N_D values) can be calculated by Mott-Schottky plots using the following equation:

$$N_D = \frac{2}{e\varepsilon_0\varepsilon}\left(\frac{dE}{d\left(\frac{1}{c^2}\right)}\right)$$

where $e = 1.6 \times 10^{-19}$ C, ε_0 = 8.86 × 10_12 F/m, and ε is the relative permittivity of the semiconductor. Thus, the N_D value is proportional to the reciprocal of the slope of the Mott-

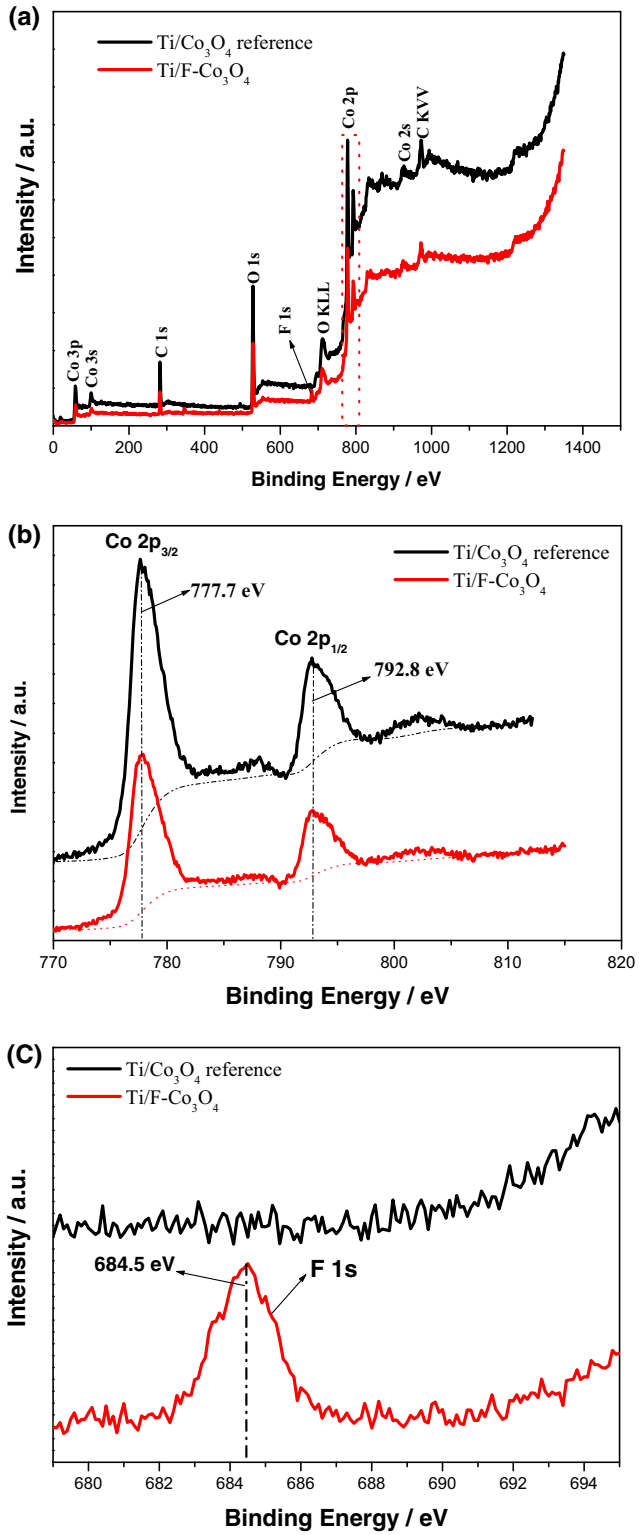

Fig. 3 XPS spectra of Ti/Co_3O_4-reference and F^- doped Ti/Co_3O_4 electrode. **a** Survey spectra. **b** Co2p spectrum. **c** F1s spectrum

Schottky plots. It is clear that from Fig. 5 a (see manuscript), the $Ti/F\text{-}Co_3O_4$-90 °C electrode has a higher carrier density (N_D) than other electrode. Thus, the $Ti/F\text{-}Co_3O_4$-90 °C electrode has lower resistance and faster charge transfer rate due to its higher N_D value, which is also beneficial to the PEC process. Figure 5 b shows the diffuse reflection spectra (DRS) of the Ti/Co_3O_4 reference and the F^- doped Ti/Co_3O_4 electrodes. It is found that all electrodes exhibited strong photo-absorption from the UV light region to visible light region. Thus, the F^- doped Ti/Co_3O_4 electrode can be used as photoanode to realize the efficient utilization of sunlight and the quick separation of induced electron-hole pairs. The steady-state polarization curves were used to evaluate the effect of hydrothermal temperature on the oxygen evolution behavior of the F^- doped Ti/Co_3O_4 electrodes, and the results were shown in Fig. 5 c. It is found that the oxygen evolution behavior of the Ti/Co_3O_4 electrode can be strongly influenced by hydrothermal temperature. Since the oxygen evolution potential (OEP) is influenced by the binding energy of intermediates (such as •OOH, •OH, and •O) with the electrode surface [46], the OEP difference of the F^- doped Ti/Co_3O_4 electrodes prepared under various hydrothermal temperatures can be ascribed so that the hydrothermal temperature influenced the surface characteristics of Ti/Co_3O_4 electrode [47, 48]. It is well known that high OEP can effectively suppress the side reaction of oxygen evolution, and improve the generation of hydroxyl radicals. Thus, the F^- doped Ti/Co_3O_4 electrode prepared by hydrothermal route at 90 °C will provide the higher current efficiency for formation of hydroxyl radicals due to their higher OEP, which is beneficial to organic oxidation by hydroxyl radicals. Herein, we also evaluated the effect of hydrothermal temperature on the cyclic voltammetry behavior of the F^- doped Ti/Co_3O_4 electrodes, and estimated the electrochemical active area or the number of active sites by using the voltammetric charge quantity (q^*) of each electrodes [49]. The voltammetric charges (q^*) corresponding to active surface areas can be determined by integrating the area of the cyclic voltammetric curve (j–E). As shown in Fig. 5 d, it can be seen that the F^- doped Ti/Co_3O_4 electrode prepared by hydrothermal route at 90 °C exhibited larger integrated area of the cyclic voltammetric curve than other Ti/Co_3O_4 electrodes.

The interfacial charge transfer properties of the F^- doped Ti/Co_3O_4 electrodes were evaluated by impedance spectroscopy. The Nyquist plots of the F^- doped Ti/Co_3O_4 electrodes were shown in Fig. 6. The EIS data were fitted by the equivalent circuit (seeing the inset of Fig. 6), where R_s, R_{ct}, and C_{dl} are the solution resistance (R_s) between working electrode and reference electrode, the charge transfer resistance (R_{ct}) of the redox reaction, and the capacitance (C_{dl}) of the electrode surface in parallel with the R_{ct}, respectively. It is found that the F^- doped Ti/Co_3O_4 electrode prepared by hydrothermal route at 90 °C has smaller R_{ct} value than other F^- doped Ti/Co_3O_4 electrodes, indicating a much faster charge transfer and superior electrochemical kinetics. Hence, the dramatic increase in intrinsic electrochemical properties of the $Ti/F\text{-}Co_3O_4$-90 °C can be attributed to the morphology effect of the divided Co_3O_4 NWs, which can shorten diffusion distance

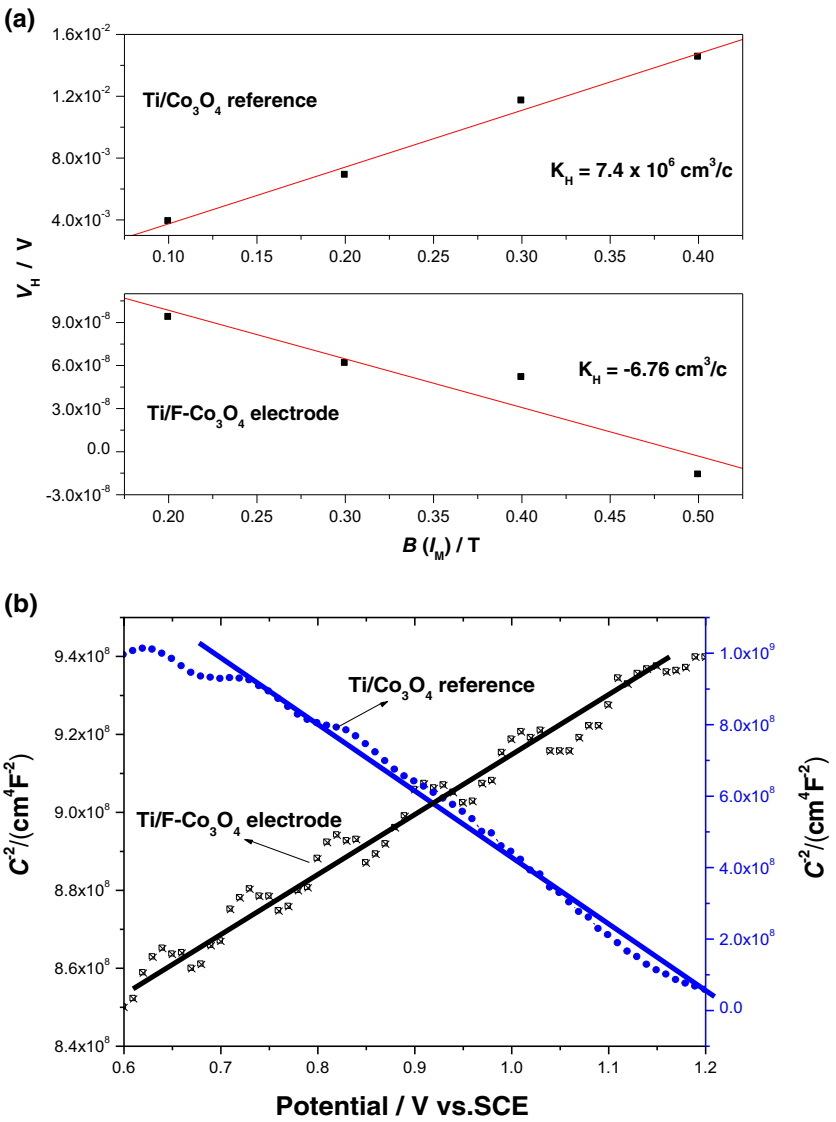

Fig. 4 Measurements of the Hall coefficient (**a**) and the Mott-Schottky plots of Ti/Co_3O_4 with or without F doping (**b**)

of charge from the surface into the inside along the radial direction [50, 51].

Figure 7 shows the photoluminescence (PL) spectra of benzoic acid solution over each electrode from different electrolysis time. As shown in Fig. 7, the F^- doped Ti/Co_3O_4 electrodes exhibited stronger fluorescence intensity during the whole period, as compared with that of Ti/Co_3O_4 reference. Especially, the $Ti/F\text{-}Co_3O_4$-90 °C electrode showed highest fluorescence intensity during the whole period. As we have known, the hydroxyl radical (•OH) is responsible for indirect electrochemical degradation of contaminants. Thus, the generation ability of the hydroxyl radical (•OH) over each electrode is proportional to their electrocatalytic activity. The PL results indicated that the F^- doped Ti/Co_3O_4 electrodes have high current efficiency of hydroxyl radical formation. Based on above mentions, we can conclude that the F^- doped Ti/Co_3O_4 electrode will exhibit excellent degradation efficiency for degradation of contaminants during the PEC process.

Figure 8 a demonstrates the photoelectrocatalytic decolorization rate of reactive Brilliant Blue (KN-R) over each electrode. As shown in Fig. 8 a, the F^- doped Ti/Co_3O_4 electrodes showed better decolorization efficiency than the Ti/Co_3O_4-reference, and the $Ti/F\text{-}Co_3O_4$-90 °C sample had the highest decolorization efficiency. It can be explained by the fact that the F^- doped Ti/Co_3O_4 electrodes have high oxygen evolution potential, low resistance, fast charge transfer rate, and large active areas. Especially, the architecture of Co_3O_4 NWs is beneficial for the fast ion and electron transportation, and good electrolyte infiltration, leading to the improved photoelectrochemical activity [52–55]. To better understand the photo-electrocatalytic (PEC) process of the F^- doped Ti/Co_3O_4 electrode, the linear scanning voltammetry behavior of the F^- doped Ti/Co_3O_4 electrode was investigated in the

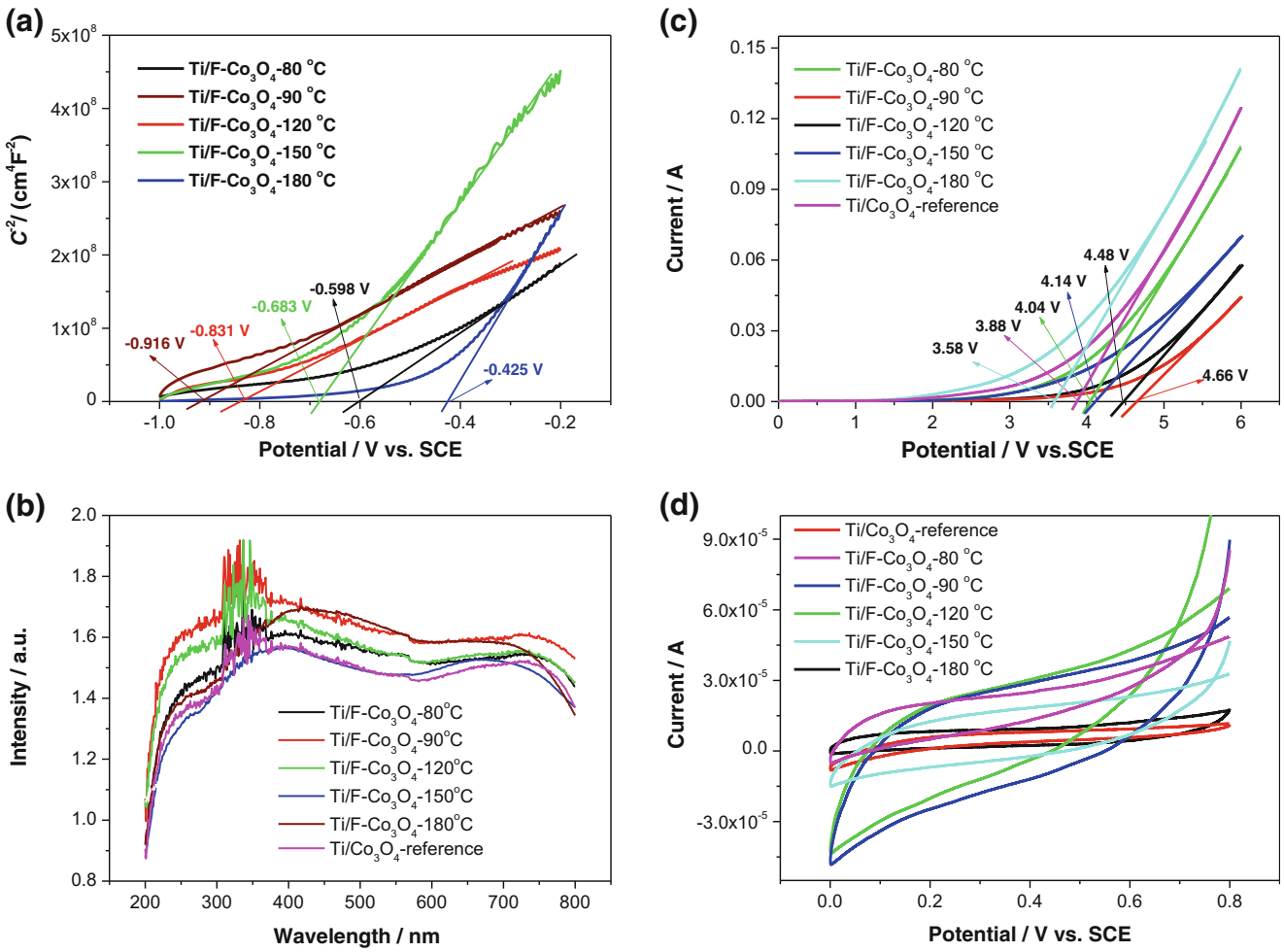

Fig. 5 (**a**) Mott-Schottky plots, (**b**) light absorption, (**c**) steady-state polarization curves in 0.1 mol L^{-1} Na_2SO_4 solution without light (the potential was swept from 0.0 to 6.0 V vs. SCE), and (**d**) cyclic voltammograms for Ti/Co_3O_4-reference and F^- doped Ti/Co_3O_4 electrode

solution with or without KN-R (see Fig. 8b). As shown in Fig. 8 b, the positive scan did not exhibit any anodic peak prior to the oxygen evolution potential in the blank solution. However, one anodic peak at about 2.0 V prior to the oxygen evolution potential can be observed while KN-R was added into the blank solution, and that the intensity of the anodic peak enhanced with the increase of KN-R content. Obviously, the anodic peak located at about 2.0 V corresponds to the direct oxidation process of KN-R [56]. Furthermore, the comparison among electrocatalytic (EC), photocatalytic (PC), and photoelectrocatalytic (PEC) process under various electrolysis conditions was performed (see Fig. 8c). As can be seen from Fig. 8 c, the photo-anode did not exhibit observable EC activity when electrolysis conditions operated at 1.5 V because the direct electrochemical oxidation of the organic pollutant occurred at 2.0 V. When the electrolysis voltage reached (or exceeded) 2.0 V, the EC activity became more and more notable, which indicated that the indirect electro-oxidation of the organic pollutant is major at high potential owing to the formation of the reactive oxygen intermediates (such as hydroxyl radicals and ozone). Furthermore, it is also found that the PEC process for the decolorization of KN-R is higher than the sum of both EC and PC at high anodic potential (see Fig. 8c). The higher decolorization efficiency of the PEC process can be attributed to a decrease of the recombination rate for photogenerated electrons/holes by applying a positive potential ("bias") across the photoanode. Interestingly, the promotion effect gradually enhances with the increase of "bias." It is well known that the reactive active species (such as superoxide radical ($O_2^{\bullet-}$), hole (h^+), ozone (O_3), and hydroxyl radical (•OH)) is responsible for the degradation of organic pollutant in photoelectrocatalytic process. Therefore, the generation of reactive active species was investigated using different types of scavengers and ultraviolet spectra analysis. A certain amount of scavengers (4.0 mmol/L) of EDTA-$2Na^+$ (for quenching the hole), isopropanol alcohol (for quenching •OH), and L-ascorbic acid (for quenching $O_2^{\bullet-}$) were added to the reaction mixture containing KN-R to subject

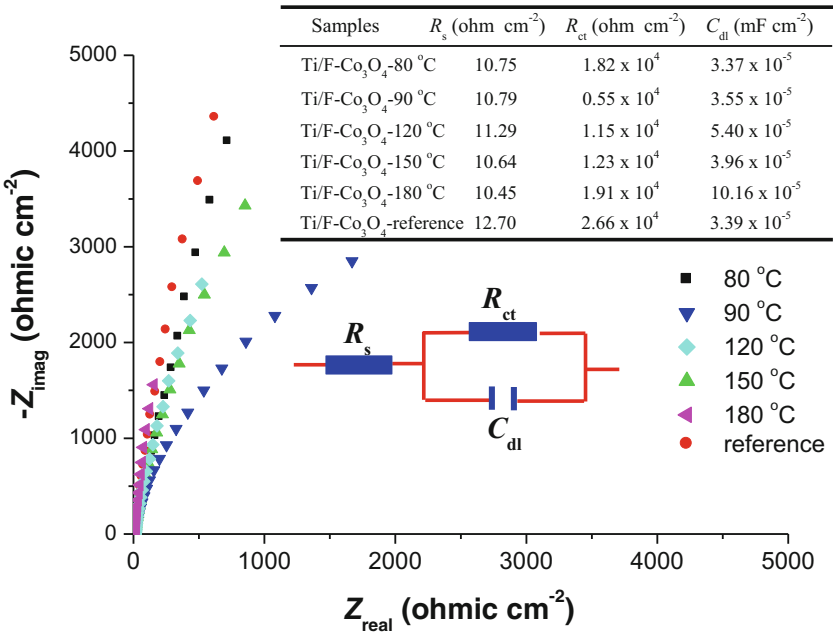

Fig. 6 Nyquist plots of the Ti/Co_3O_4-reference and F^- doped Ti/Co_3O_4 electrodes at open circuit potential. The inset shows the equivalent circuit for the electrochemical cell, where R_s, R_{ct}, and C_{dl} are the series resistance, charge transfer resistance, and capacitance of the electrode surface, respectively

degradation by photoelectrocatalysis. It can be seen from Fig. 8 d that the degradation of reactive Brilliant Blue KN-R is derived from the combined action of these active species in the photoelectric process. Furthermore, the stability of the F^- doped Ti/Co_3O_4 electrode (Ti/F-Co_3O_4-90 °C) was also evaluated by the recycling degradation experiments of the reactive Brilliant Blue KN-R. As shown in Fig. 8 e, Ti/F-Co_3O_4-90 °C electrode still exhibited a considerable removal rate (about 64%) of reactive Brilliant Blue KN-R after five cycles. The above results indicated that the F^- doped Ti/Co_3O_4 electrode would be a potential PEC electrode for practical application.

Based on above results, the possible PEC processes were described as follows (see Scheme 1): Firstly, the electrons (e^-) in valence band of Co_3O_4 under light irradiation could be excited to the conduction band, leaving the holes (h^+) in valence band of Co_3O_4. When applying an anodic bias potential to the semiconductor (applied potential is greater than the flat band potential), there will be an increase of band bending. Thus, electrons in the conduction band are flown through the counter electrode via the external circuit, and the holes are transferred into the surface. Furthermore, we well know that the work

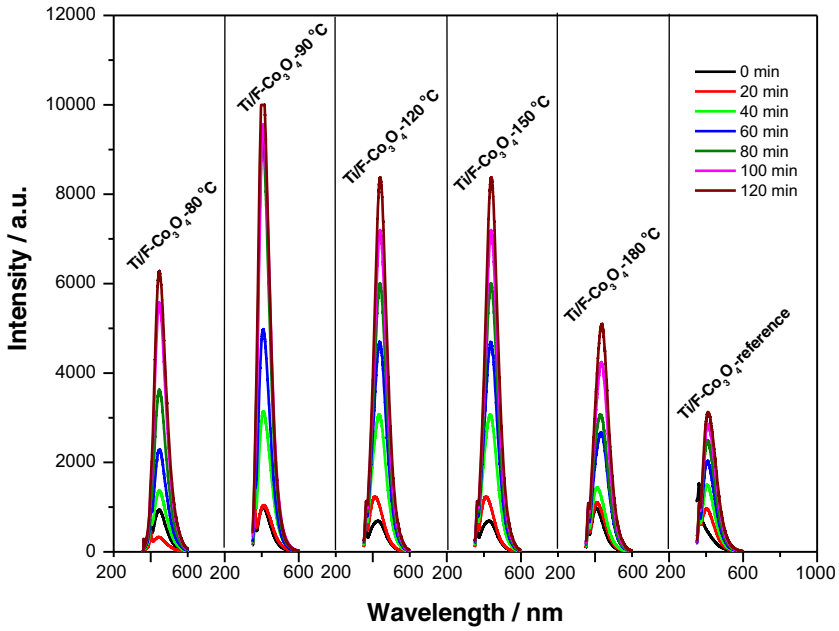

Fig. 7 Fluorescence spectra of benzoic acid (200 mgL^{-1} benzoic acid and 0.5 molL^{-1} Na_2SO_4 as supporting electrolyte) over the Ti/Co_3O_4-reference and F^- doped Ti/Co_3O_4 electrodes during photoelectrolysis

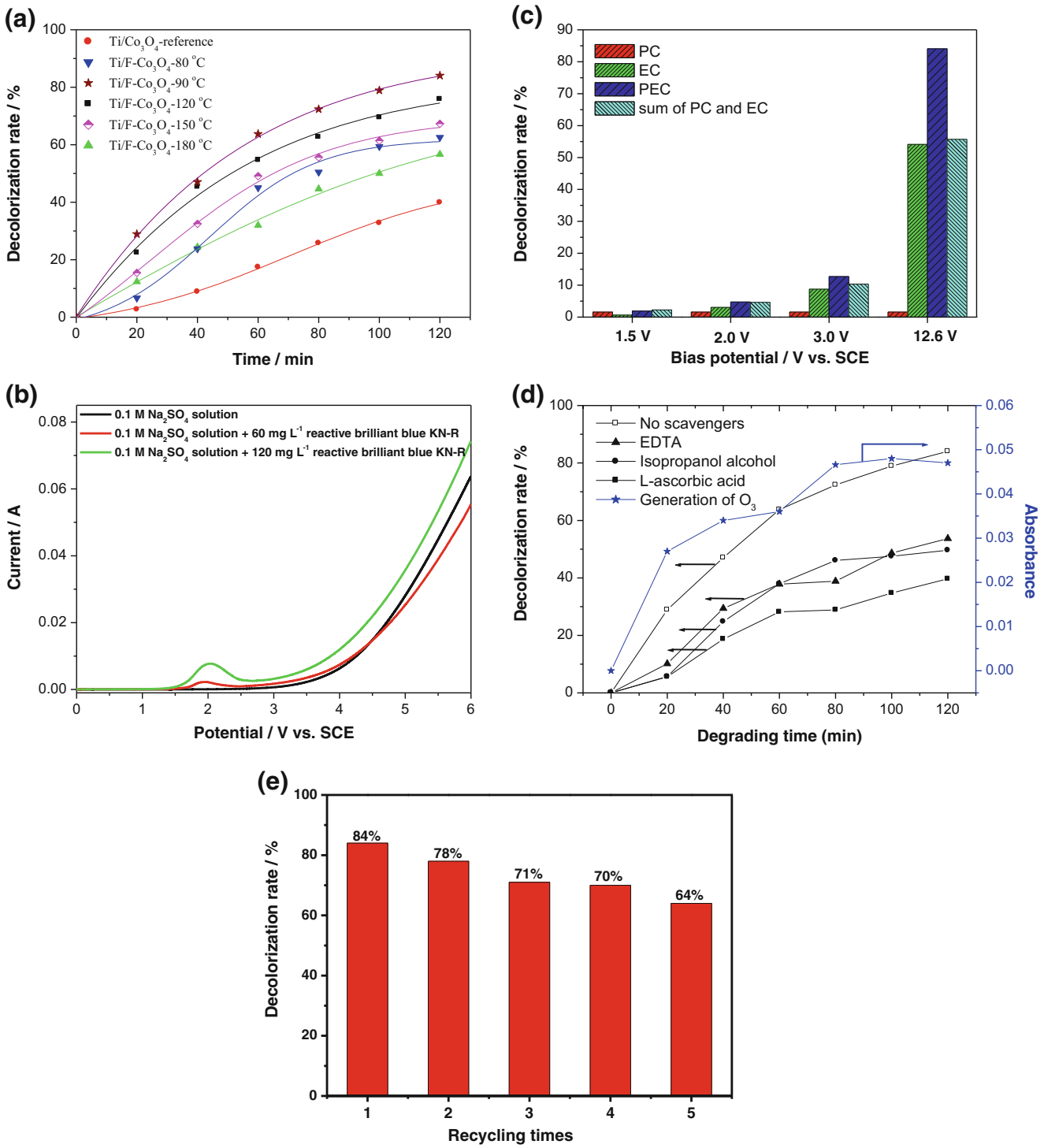

Fig. 8 (**a**) Decolorization efficiencies of KN-R over the Ti/Co_3O_4-reference and F^- doped Ti/Co_3O_4 electrodes, (**b**) linear scanning voltammograms of the F^- doped Ti/Co_3O_4 electrode, (**c**) the effect of the applied bias on the degradation rate of KN-R over the F^- doped Ti/Co_3O_4 electrode, (**d**) the evaluation of active species using various scavengers, and (**e**) the recycling of experiments of the F^- doped Ti/Co_3O_4 electrodes for five cycles

function of the Co_3O_4 ($\phi_s = 4.5$ eV) exceeds that of the substrate Ti ($\phi_m = 4.33$ eV). Thus, the bands are bent downwards, giving an ohmic contact. The band-bending causes no impediment to the motion of the induced electrons from the conduction band of Co_3O_4 into the metal Ti. And then, the electrons were faster moved to the external circuit via electric field, and the induced charge carriers were effectively separated.

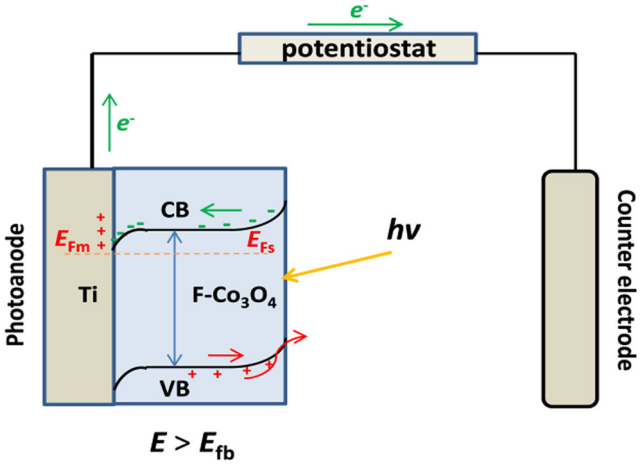

Scheme 1 Charge transfer mechanism in the F^- doped Ti/Co_3O_4 electrode under PEC process

Conclusions

In this work, we demonstrated that the F doped Ti/Co_3O_4 electrode with *n*-type characteristics can be prepared by the hydrothermal process. The tailoring of the Co_3O_4 morphology is realized by controlling hydrothermal temperature. It is found that the F^- doping can cause the formation of more regular architectures composed of Co_3O_4 nanowires. Moreover, the morphology of Co_3O_4 coatings is converted from nanowires to solid prisms with enhancing hydrothermal temperature. The morphology of Co_3O_4 coatings influences strongly the PEC activity of electrodes (the solid prism-like Co_3O_4 coatings possess a lower PEC activity). Nevertheless, the F^- doped Ti/Co_3O_4 electrodes showed high oxygen evolution potential, low resistance, fast charge transfer rate and large active area, and higher current efficiency of hydroxyl radical formation. Consequently, a very high PEC activity for F^- doped Ti/Co_3O_4 electrodes is achieved.

Funding information This work was supported by the National Natural Science Foundation of China (21875026, 21878031), the Program for Liaoning Excellent Talents in University (LR2014013), the Natural Science Foundation of Liaoning Province (No. 20170520427), and the Science and Technology Foundation of Liaoning Province (No. 201602052).

References

1. Wang L, Ke F, Zhu J (2016) Metal-organic gel templated synthesis of magnetic porous carbon for highly efficient removal of organic dyes. Dalton Trans 45(11):4541–4547
2. Martinez-Huitle CA, Ferro S (2006) Electrochemical oxidation of organic pollutants for the wastewater treatment: direct and indirect processes. Chem Soc Rev 35(12):1324–1340
3. Korbahti BK, Tanyolac A (2008) Electrochemical treatment of simulated textile wastewater with industrial components and Levafix Blue CA reactive dye: optimization through response surface methodology. J Hazard Mater 151(2-3):422–431
4. Barredo-Damas S, Iborra-Clar MI, Bes-Pia A, Alcaina-Miranda MI, Mendoza-Roca JA, Iborra-Clar A (2005) Study of preozonation influence on the physical-chemical treatment of textile wastewater. Desalination 182(1-3):267–274
5. Feng Y, Yang L, Liu J, Logan BE (2016) Electrochemical technologies for wastewater treatment and resource reclamation. Environ Sci: Wat Res Technol 2:800–831
6. Moussavi G, Mahmoudi M (2009) Removal of azo and anthraquinone reactive dyes from industrial wastewaters using MgO nanoparticles. J Hazard Mater 168(2-3):806–812
7. Gong D, Zhu J, Lu B (2016) RuO_2@Co_3O_4 heterogeneous nanofibers: a high-performance electrode material for supercapacitors. RSC Adv 6(54):49173–49178
8. He ZQ, Huang CX, Wang Q, Jiang Z, Chen JM, Song S (2011) Preparation of a praseodymium modified Ti/SnO_2-Sb/PbO_2 electrode and its application in the anodic degradation of the A1zo dye acid black 194. Environ Sci: Wat Res Technol 6:4341–4354
9. Polcaro AM, Palmas S, Renoldi F, Mascia M (1999) On the performance of Ti/SnO_2 and Ti/PbO_2 anodes in electrochemical degradation of 2-chlorophenol for wastewater treatment. J Appl Electrochem 29(2):147–151
10. Dai Q, Shen H, Xia Y, Chen F, Wang J, Chen J (2013) The application of a novel Ti/SnO_2–Sb_2O_3/PTFE-La-Ce-β-PbO_2 anode on the degradation of cationic gold yellow X-GL in sono-electrochemical oxidation system. Sep Purif Technol 104:9–16
11. Haidar M, Dirany A, Sires I, Oturan N, Oturan MA (2013) Electrochemical degradation of the antibiotic sulfachloropyridazine by hydroxyl radicals generated at a BDD anode. Chemosphere 91(9):1304–1309
12. Dan YY, Zhang L, Chen LZ, Yue HJ, Lin HB, Lu HY (2014) Preparation of PbO_2/nano-WO_3 composite electrodeposition Ti substrate by composite electrodeposition and its oxygen evolution activity. Chem J Chin Univ 35:2632–2637
13. Geng R, Zhao GH, Liu MC, Lei YZ (2010) In situ ESR study of hydroxyl radical generation on a boron doped diamond film electrode surface. Acta Phys -Chim Sin 26:1493–1498
14. Velichenko AB, Girenko DV, Amadelli R, Danilov FI (1998) Effect of fluoride ions on electrodeposition of lead dioxide at the gold electrode. Russ JEl ectrochem 34:298–301
15. Velichenko AB, Girenko DV, Kovalyov SV, Gnatenko AN, Amadelli R, Danilov FI (1998) Lead dioxide electrodeposition and its application: influence of fluoride and iron ions. J Electroanal Chem 454(1-2):203–208
16. Amadelli R, Armelao L, Velichenko AB, Nikolenko NV, Girenko DV, Kovalyov SV, Danilov FI (1999) Oxygen and ozone evolution at fluoride modified lead dioxide electrodes. Electrochim Acta 45:713–720
17. Velichenko AB, Amadelli R, Baranova EA, Girenko DV, Danilov FI (2002) Electrodeposition of Co-doped lead dioxide and its physicochemical properties. J Electroanal Chem 527(1-2):56–64
18. Mojumder N, Sarker S, Abbas SA, Tian Z, Subramanian V (2014) Photoassisted enhancement of the electrocatalytic oxidation of formic acid on platinized TiO_2 nanotubes. ACS Appl Mater Interfaces 6(8):5585–5594
19. Akira F, Rao TN, Tryk DA (2000) Titanium dioxide photocatalysis. Photochem Photobio C: Photochem Rev 1:1–21
20. Vlyssides AG, Karlis PK, Rori N, Zorpas AA (2002) Electrochemical treatment in relation to pH of domestic wastewater using Ti/Pt electrodes. J Hazard Mater B 95(1-2):215–226
21. Kong Y, Wang Z, Wang Y, Yuan J, Chen Z (2011) Degradation of methyl orange in artificial wastewater through electrochemical oxidation using exfoliated graphite electrode. New Carbon Mater 26(6):459–464
22. Shen YM, Li F, Li SF, Liu DB, Fan LH, Zhang Y (2012) Electrochemically enhanced photocatalytic degradation of organic

pollutant on β-PbO_2 -TNT/Ti/TNT bifunctional electrode. J Electrochem Sci Technol 7:8702–8712
23. Li PQ, Zhao GH, Cui X, Zhang YG, Tang YT (2009) Constructing stake structured TiO_2-NTs/Sb-doped SnO_2 electrode simultaneously with high electrocatalytic and photocatalytic performance for complete mineralization of refractory aromatic acid. J Phys Chem C 113(6):2375–2383
24. Li PQ, Zhao GH, Li MF, Cao TH, Cui X, Li DM (2012) Design and high efficient photoelectric-synergistic catalytic oxidation activity of 2D macroporous SnO_2/1D TiO_2 nanotubes. Appl Catal B Environ 111:578–585
25. He H, Zhang C, Liu T, Cao Y, Wang N, Guo Z (2016) Thermoelectric–photoelectric composite nanocables induced a larger efficiency in dye-sensitized solar cells. J Mater Chem A 4(24):9362–9369
26. Raj BGS, Wu JJ, Asiri AM, Anandan S (2016) Hybrid SnO_2-Co_3O_4 nanocubes prepared via $CoSn(OH)_6$ intermediate through sonochemical route for energy storage applications. RSC Adv 6: 33361–33368
27. Huang X, Cao T, Liu M, Zhao G (2013) Synergistic photoelectrochemical synthesis of formate from CO_2 on {$1\bar{2}\bar{1}$} hierarchical Co_3O_4. J Phys Chem C 117(50):26432–26440
28. Lee CY, Lee K, Schmuki P (2013) Anodic formation of self-organized cobalt oxide nanoporous layer. Angew Chem Int Ed 52(7):2077–2081
29. Lee CY, Su Z, Lee K, Tsuchiya H, Schmuki P (2014) Self-organized cobalt fluoride nanochannel layers used as a pseudocapacitor material. Chem Commun 50(53):7067–7070
30. Li M, El-Kady MF, Hwang JY, Kowal MD, Marsh K, Wang H, Zhao Z, Kaner RB (2018) Embedding hollow Co_3O_4 nanoboxes into a three-dimensional macroporous graphene framework for high-performance energy storage devices. Nano Res 11(5):2836–2846
31. Liu X, Chen S, Yu J, Zhang W, Dai Y, Zhang S (2015) Ni-enhanced Co_3O_4 nanoarrays grown in situ on a Cu substrate as integrated anode materials for high-performance Li-ion batteries. RSC Adv 5:7388–7394
32. Shi P, Dai X, Zheng H, Li D, Yao W, Hu C (2014) Synergistic catalysis of Co_3O_4 and graphene oxide on Co_3O_4/GO catalysts for degradation of Orange II in water by advanced oxidation technology based on sulfate radicals. Chem Eng J 240:264–270
33. Wu JB, Li ZG, Huang XH, Lin Y (2013) Porous Co_3O_4/NiO core/shell nanowire array with enhanced catalytic activity for methanol electro-oxidation. J Power Sources 224:1–5
34. Zhao J, Zhu C, Lu J, Hu C, Peng S, Chen T (2014) Electro-catalytic degradation of bisphenol A with modified Co_3O_4/β-PbO_2/Ti electrode. Electrochim Acta 118:169–175
35. Fantini M, Torrian I (1986) The compositional and structural properties of sprayed SnO_2: F thin films. Thin Solid Films 138(2):255–265
36. zhao GH, Zhang YG, Lei YZ, Lv BY, Gao JX, Zhang YN, Li DM (2010) Fabrication and electrochemical treatment application of a novel lead dioxide anode with superhydrophobic surfaces, high oxygen evolution potential, and oxidation capability. Environ Technol 44:1754–1759
37. Bhardwaj A, Gupta BK, Raza A, Sharma AK, Agnihotri OP (1981-1982) Fluorine-doped SnO_2films for solar cell application. Sol Energ Mater Sol C 5:39–49
38. van der Pauw LJ (1958) A method of measuring specific resistivity and Hall effect of discs of arbitrary shape. Philips Res Rep 13:1–9
39. Ding Y, Wang Y, Su L, Bellagamba M, Zhang H, Lei Y (2010) Electrospun Co_3O_4 nanofibers for sensitive and selective glucose detection. Biosens Bioelectron 26(2):542–548
40. Sung HK, Oh SY, Park C, Kim Y (2013) Colorimetric detection of Co^{2+} ion using silver nanoparticles with spherical, plate, and rod shapes. Langmuir 29(28):8978–8982
41. Barreca D, Bekermann D, Comini E, Devi A, Fischer RA, Gasparotto A, Gavagnin M, Maccato C, Sada C, Sberveglieri G, Tondello E (2011) Plasma enhanced-CVD of undoped and fluorine-doped Co_3O_4 nanosystems for novel gas sensors. Sensors Actuators B Chem 160:79–86
42. Gasparotto A, Barreca D, Bekermann D, Devi A, Fischer RA, Fornasiero P, Gombac V, Lebedev OI, Maccato C, Montini T, Tendeloo GV, Tondello E (2011) F-Doped Co_3O_4 photocatalysts for sustainable H_2 generation from water/ethanol. J Am Chem Soc 133(48):19362–19365
43. Kong DS, Lu WH, Feng YY, Bi SW (2009) Advances and some problems in electrocatalysis of DSA electrodes. Prog Chem 21: 1107–1117
44. Harrington SP, Devine TM (2008) Analysis of electrodes displaying frequency dispersion in Mott-Schottky tests. J Electrochem Soc 155(8):C381–C386
45. Wang Z, Yang CY, Lin TQ, Hao Y, Chen P, Wan DY, Xu FF, Huang FQ, Lin JH, Xie XM, Jiang MH (2013) Visible-light photocatalytic, solar thermal and photoelectrochemical properties of aluminium-reduced black titania. Energy Environ Sci 6(10):3007–3014
46. García-Mota M, Vojvodic A, Metiu H, Man IC, Su HY, Rossmeisl J, Nørskov JK (2011) Tailoring the activity for oxygen evolution electrocatalysis on rutile TiO_2(110) by transition-metal substitution. ChemCatChem 3(10):1607–1611
47. Roy N, Sohn Y, Leung KT, Pradhan D (2014) Engineered electronic states of transition metal doped TiO_2 nanocrystals for low overpotential oxygen evolution reaction. J Phys Chem C 118(51):29499–29506
48. Liu B, Chen HM, Liu C, Andrews SC, Hahn C, Yang P (2013) Large-scale synthesis of transition-metal-doped TiO_2 nanowires with controllable over potential. J Am Chem Soc 135(27):9995–9998
49. Zhang L, Xu L, He J, Zhang J (2014) Preparation of Ti/SnO_2-Sb electrodes modified by carbon nanotube for anodic oxidation of dye wastewater and combination with nanofiltration. Electrochim Acta 117:192–201
50. Wang Y, Xia H, Lu L, Lin JY (2010) Excellent performance in lithium-ion battery anodes: rational synthesis of $Co(CO_3)_{0.5}(OH)0.11H_2O$ nanobelt array and its conversion into mesoporous and single-crystal Co_3O_4. ACS Nano 4(3):1425–1432
51. Mai L, Tian X, Xu X, Chang L, Xu L (2014) Nanowire electrodes for electrochemical energy storage devices. Chem Rev 114(23): 11828–11862
52. Li XL, Li XM, Yang WJ, Chen XH, Li WL, Luo BB, Wang KL (2014) Preparation of 3D PbO_2 nanospheres@SnO_2 nanowires/Ti electrode and its application in methyl orange degradation. Electrochim Acta 146:15–22
53. Chen T, Li XW, Qiu CC, Zhu WC, Ma HY, Chen SH, Meng O (2014) Electrochemical sensing of glucose by carbon cloth-supported Co_3O_4/PbO_2 core-shell nanorod arrays. Biosens Bioelectron 53:200–206
54. Wang GL, Cao DX, Yin CL, Gao YY, Yin JL, Cheng L (2009) Nickel foam supported-Co_3O_4 nanowire arrays for H_2O_2 electroreduction. Chem Mater 21(21):5112–5118
55. He JF, Peng YH, Sun ZH, Cheng WR, Liu QH, Feng YJ, Jiang Y, Hu FC, Pan ZY, Bian Q, Wei SQ (2014) Realizing high water splitting activity on Co_3O_4 nanowire arrays under neutral environment. Electrochim Acta 119:64–71
56. Amadelli R, Samiolo L, Battisti AD, Velichenko AB (2011) Electro-oxidation of some phenolic compounds by electrogenerated O_3 and by direct electrolysis at PbO_2 anodes. J Electrochem Soc 158:87–92